Aust. J. Phys., 1995, **48**, 217–31

Photoelectron Spectroscopy of Solids using Synchrotron Radiation*

Robert Leckey and John Riley

School of Physics, Faculty of Science and Technology,
La Trobe University, Bundoora, Vic. 3083, Australia.

Abstract

A brief review of the technique of angle-resolved photoelectron spectroscopy as used in conjunction with synchrotron radiation is given. Examples of the use of the technique which emphasise the collection of full-hemisphere data are presented, covering the determination of Fermi surface topology and photoelectron diffraction/holography. An example of an investigation of quantum size effects and of the use of magnetic circular dichroism to explore the interaction of spin–orbit and exchange effects in iron is also provided.

1. Introduction

Photoelectron spectroscopy, in conjunction with synchrotron radiation, has developed over the past decade into a mature technique for the elucidation of the electronic structure of materials (Hufner 1994). The determination of surface structural information by the photoemission method is as yet less well developed, but significant progress is currently being made (Chambers 1992).

In the past, the major success of the technique in its angle-resolved form has been the determination of the details of the occupied band structure of metals and semiconductors. As the technique has matured, the emphasis has evolved to cover an increasing interest in using variants of the technique to explore the unoccupied bands, to extend the study to magnetic sub-levels, to examine the topology of the Fermi surface of metals and alloys and to investigate quantum size effects.

In this paper we will examine the technique of photoelectron spectroscopy of solids as it is practised at synchrotron radiation facilities, briefly consider the attributes of synchrotron radiation that enable the marriage of the two to be so successful, and provide examples which illustrate a few of the exciting developments that have occurred in this field in recent years.

2. Experimental Considerations

The use of photons to eject electrons from solids has a venerable history (Jenkin *et al.* 1977). In large part, the attraction of photons as the incident

* Refereed paper based on a plenary lecture given to the joint Sixth Asia Pacific Conference and Eleventh Australian Institute of Physics Congress held at Griffith University, Brisbane, July 1994.

0004-9506/95/020217$05.00

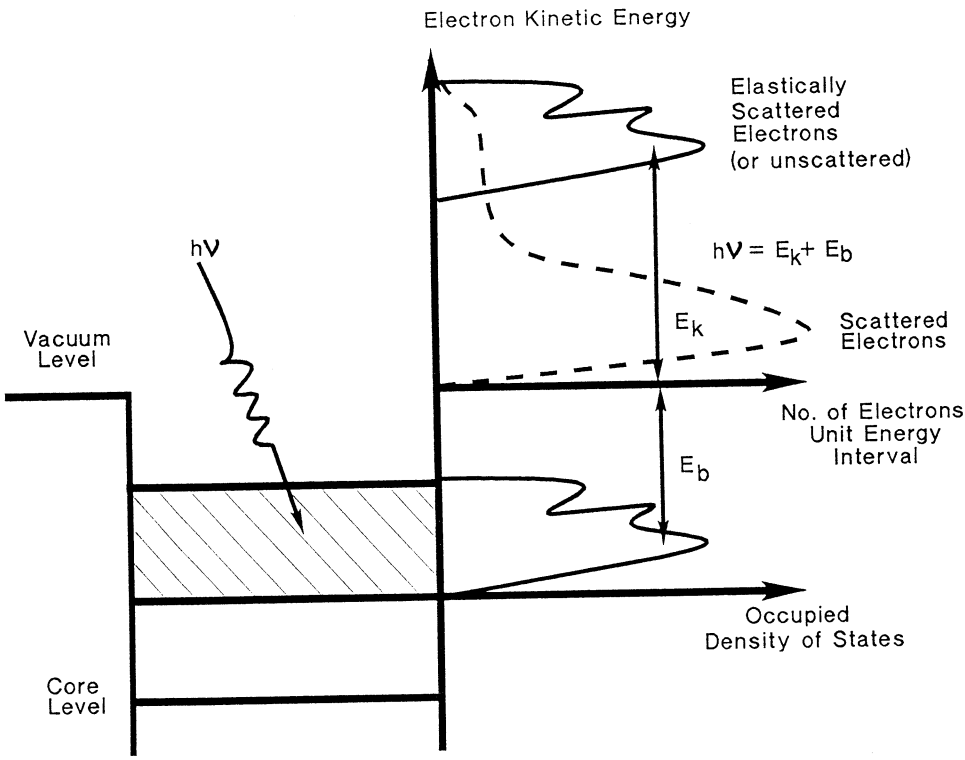

Fig. 1. Illustration of the basic mechanism of photoemission.

probe lies in the fact that, for low energies (no greater than say 500 eV), the photon transfers all its energy to the electron but there is negligible momentum transfer. By determining the kinetic energy of emission, the binding energy of the electron in the solid E_b is immediately given by the Einstein equation:

$$\hbar\nu = E_b + E_k + \Phi, \tag{1}$$

where E_k is the electron kinetic energy and Φ is the work function. Since the probability of photoexcitation is proportional to the product of the densities of occupied and unoccupied states, the resulting spectrum can provide information about not only the location in energy of occupied states, but also their population density (see Fig. 1). If the material is crystalline, and information concerning the emission direction of the electrons is also collected, the photoemission experiment further provides an almost direct determination of the occupied $E(\boldsymbol{k})$ bandstructure of the material.

The key to understanding the previous statement lies in the recognition that the electron, once emitted from the material, is free and consequently its energy–momentum dispersion is known to be

$$E_k = \hbar^2(\boldsymbol{K} + \boldsymbol{G})^2/2m, \tag{2}$$

where the inclusion of a reciprocal lattice vector $\boldsymbol{G}$ is required to conserve momentum (Himpsel 1983). It turns out that this free-electron description is also a reasonable description of the photoexcited electron within the crystal provided the kinetic energy is greater than about 20 eV. The components of momentum parallel and normal to the crystal surface follow as

$$\hbar \boldsymbol{K}_{\mathrm{p}}(\text{internal}) = \hbar \boldsymbol{K}_{\mathrm{p}}(\text{external}) = (2mE_{\mathrm{k}})^{1/2} \sin\theta\,, \tag{3}$$

$$\hbar \boldsymbol{K}_{\mathrm{n}}(\text{external}) = 2m(E_{\mathrm{k}} + V_0)^{1/2} \cos\theta\,, \tag{4}$$

where V_0 is the inner potential.

Since, due to the presence of the surface itself, the periodicity of the crystal lattice is preserved in directions parallel to the surface but not perpendicular to it, the determination of the total momentum of the electron within the crystal requires additional information in most circumstances. This follows because although the parallel component is conserved across the interface, the perpendicular component is not and so it remains somewhat indeterminate for the internal electron state.

A rather direct determination of the band structure in the direction perpendicular to the selected surface is possible, provided that the electrons detected are only those emitted normal to the surface (Himpsel 1983). As a first example of an angle-resolved measurement of this type, typical normal emission spectra from a GaAs (001) surface are shown in Fig. 2*a*.

Fig. 2*a* illustrates the primary reason for using synchrotron radiation, namely the ability to select a desired photon energy from the continuum radiation produced at the locations of the bending magnet of the ring. The fact that the radiation is much more intense than laboratory sources is, of course, a bonus and we will see later that the polarisation of the radiation can also be most usefully exploited. An additional attribute of synchrotron radiation, namely its pulsed nature, has not yet been utilised to any large extent in condensed matter studies.

Synchrotron radiation, while essential for the experiments discussed here, is not without its difficulties for the user. Although the radiation produced by the source is exactly calculable, it is delivered to the user via a monochromator-beamline, whose characteristics need to be carefully integrated into the design of any experiment. Some properties of a particular beamline at the Berlin facility (Petersen *et al.* 1992) are shown in Fig. 3, from which the significant effects of contamination on the optical elements may clearly be seen. Although this beamline has excellent photon energy resolution, this is achieved at the expense of intensity, with the result that users continue to request the provision of even brighter sources. Additional brightness can be produced by the use of undulators placed in straight sections of the source and, indeed, the current generation of new synchrotron sources is largely designed to accommodate large numbers of such devices with a smaller number of bending magnets being used to close the trajectory. An obvious disadvantage for Australian users of synchrotron radiation is the travel time involved in accessing such sources, together with the costs of instrumentation and connection.

3. Band Structure Determination

Returning to Fig. 2*a*, certain peaks in the set of energy distributions shown clearly disperse in binding energy as the incident photon energy (and hence the

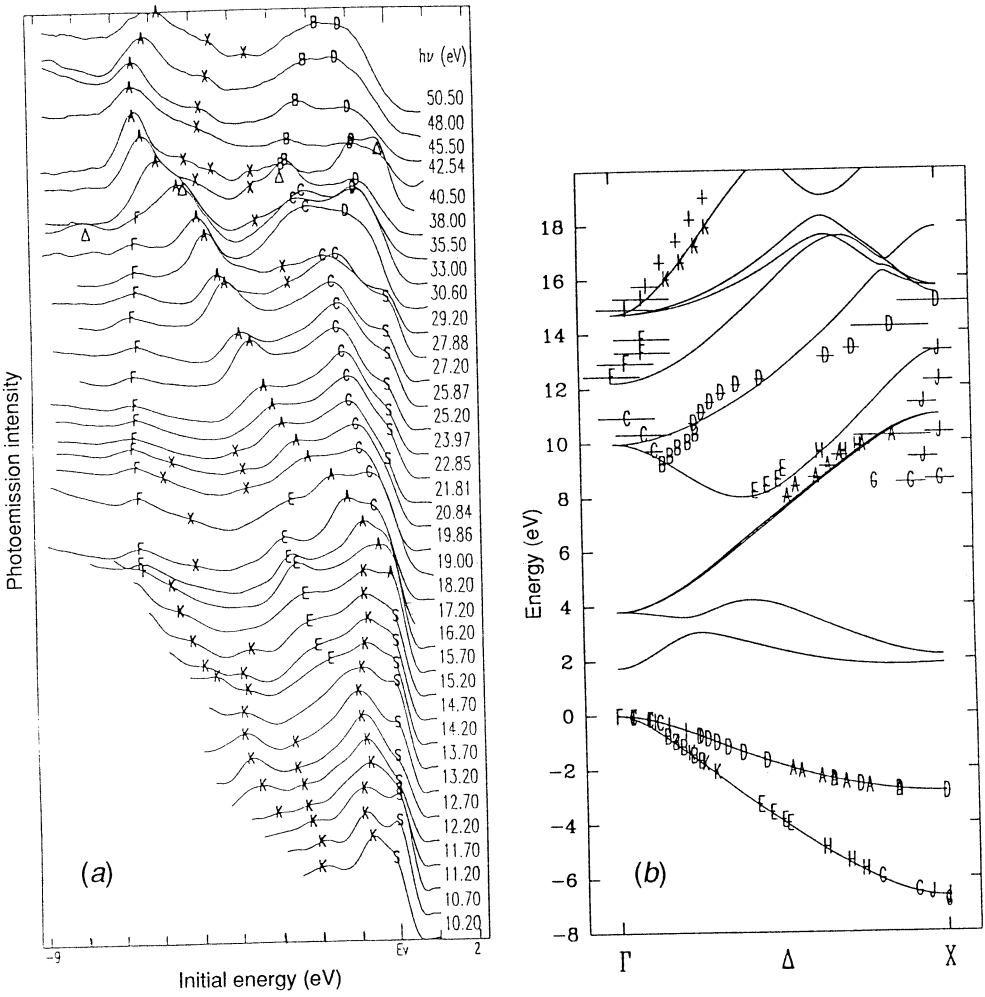

Fig. 2. (*a*) Normal emission energy distribution curves from GaAs (001) acquired using a range of photon energies. (*b*) Conduction band structure of GaAs (001) derived from data including those shown in (*a*). Letter symbols are experiment and the curves theory. (From Zhang *et al.* 1993.)

momentum of the electron) is varied. These peaks involve transitions from band states along the perpendicular direction and their dispersion can be determined relatively unambiguously from data such as that of Fig. 2*a*. Details of this procedure and a survey of results for semiconductors may be found in Leckey and Riley (1992), which also includes a critique of the method. Since the valence states may now be calculated with significantly more confidence than the higher conduction bands, we prefer to invert the standard photoemission technique and use the experimental data to determine the conduction band states. That is, we assume a calculated set of valence states rather than assume the validity of the free-electron approximation for the conduction band states, as is usually done whenever the valence band states are to be investigated. An example of this procedure is shown in Fig. 2*b* (Zhang *et al.* 1993).

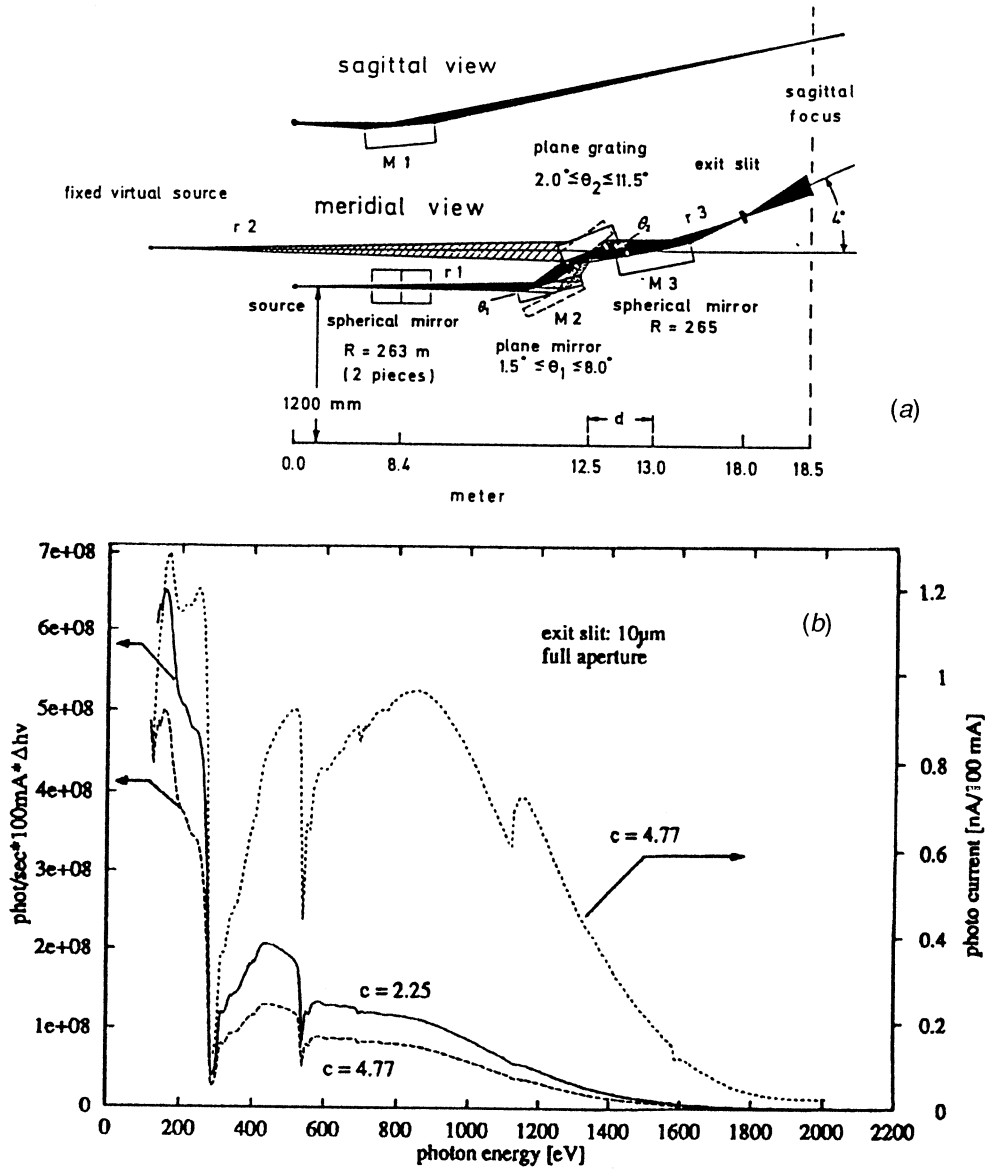

Fig. 3. (*a*) Details of the optical arrangement of the High Energy Plane Grating Monochromator (HE PGM-3) at the Berlin Synchrotron Radiation Source (BESSY). (From Petersen *et al.* 1992.) (*b*) Variation of the photon flux as a function of photon energy for the HE PGM-3 beamline under conditions of significant surface contamination. (From Petersen *et al.* 1991.) The parameter c may be chosen to enhance either resolution or flux by means of a moveable exit slit. The photocurrent detected by a GaAs photodiode, placed to intercept the beam, is also shown.

The peak labelled S in Fig. 2*a* does not show energy dispersion as a function of photon energy and is consequently a good candidate for identification as a surface state. Surface states involve solutions of the Schrödinger equation specific to the immediate surface region: they exhibit dispersion in directions parallel to the crystal surface but not perpendicular to it, due to their spatial confinement close to the surface region. This in turn implies no dispersion as the photon

energy is altered. Such surface electronic states are of particular importance in catalysis and in the production of integrated circuits, for example.

An example of how surface states may dominate the electronic structure of a material is illustrated in Fig. 4*b*, which shows the dispersion of the valence band of GaAs(001) contrasted with comparable data (Fig. 4*a*) for the conduction band of Cu(111). In the case of Cu, the relatively dispersionless 3d bands dominate the data and a strongly dispersing portion of the 4s band may be seen approaching the Fermi level. A localised surface state is also visible at the Fermi energy, and appears in this diagram close to normal emergence. In the GaAs case, essentially all the dispersion close to the top of the valence band is due to the presence of the surface state labelled S in Fig. 2*a*. This clearly dominates the structure due to the bulk bands which may, however, be observed at larger binding energies in Fig. 4*b* and more clearly in Fig. 4*c*.

The continuous lines in Fig. 4*c* are the loci of transitions to be expected between pairs of $E(\boldsymbol{k}_{\mathrm{par}}, \boldsymbol{k}_{\mathrm{perp}})$ surfaces whose energies are separated by the photon energy, as calculated using an *ab initio* scheme (Christensen 1984). The details of this data processing may be found in the thesis by Cai (1992), but it is of importance here to note that such an analysis probes the agreement between experiment and theory over a large part of the Brillouin zone and not only at selected symmetry points. This follows from the fact that the experiment provides information concerning those transitions that are permitted between two *surfaces* (rather than merely two lines) in reciprocal space, each of which spans the Brillouin zone.

Fig. 4 is an example of the additional insight which may be obtained by performing a detailed angle-resolved photoemission experiment, although the data are restricted to emission in a particular azimuthal plane. The full power of an angle-resolved experiment may be seen whenever data are collected that cover the entire emission hemisphere. Examples of such experiments include those that seek to establish the topology of the Fermi surface of alloys and those that involve structural determination via photoelectron diffraction.

4. Fermi Surface Studies

By selecting those electrons whose kinetic energy (in conjunction with the selected photon energy) implies that they originate from states at the Fermi energy, and determining their intensity over the emission hemisphere, we may almost directly examine the shape of the Fermi surface in $\boldsymbol{k}$-space. This is most evident if the data are transformed from $N(\theta, \phi)$ form to $N(k_x, k_y)$ form, where k_x, k_y are the components of the electron wavevector in two orthogonal directions parallel to the surface.

Fig. 4. (*a*) Photoemission from the conduction band of Cu(111) excited by 21 eV p-polarised light. Intensity is plotted as a function of binding energy and of emission angle in the [112] azimuthal plane. Note the surface state emission centred at normal emission. (*b*) Photoemission from the valence band of GaAs(110) excited by 26 eV p-polarised light. The intensity near the top of the valence band is dominated by surface state emission. (*c*) The location of peaks in the intensity distribution of (*b*) are indicated by letter symbols, while the curves are the theoretically predicted loci of strong transitions involving bulk bands. The cross-hair circles indicate the dispersion of a surface state which dominates emission near the top of the valence band. Features E and F show effects due to indirect transitions.

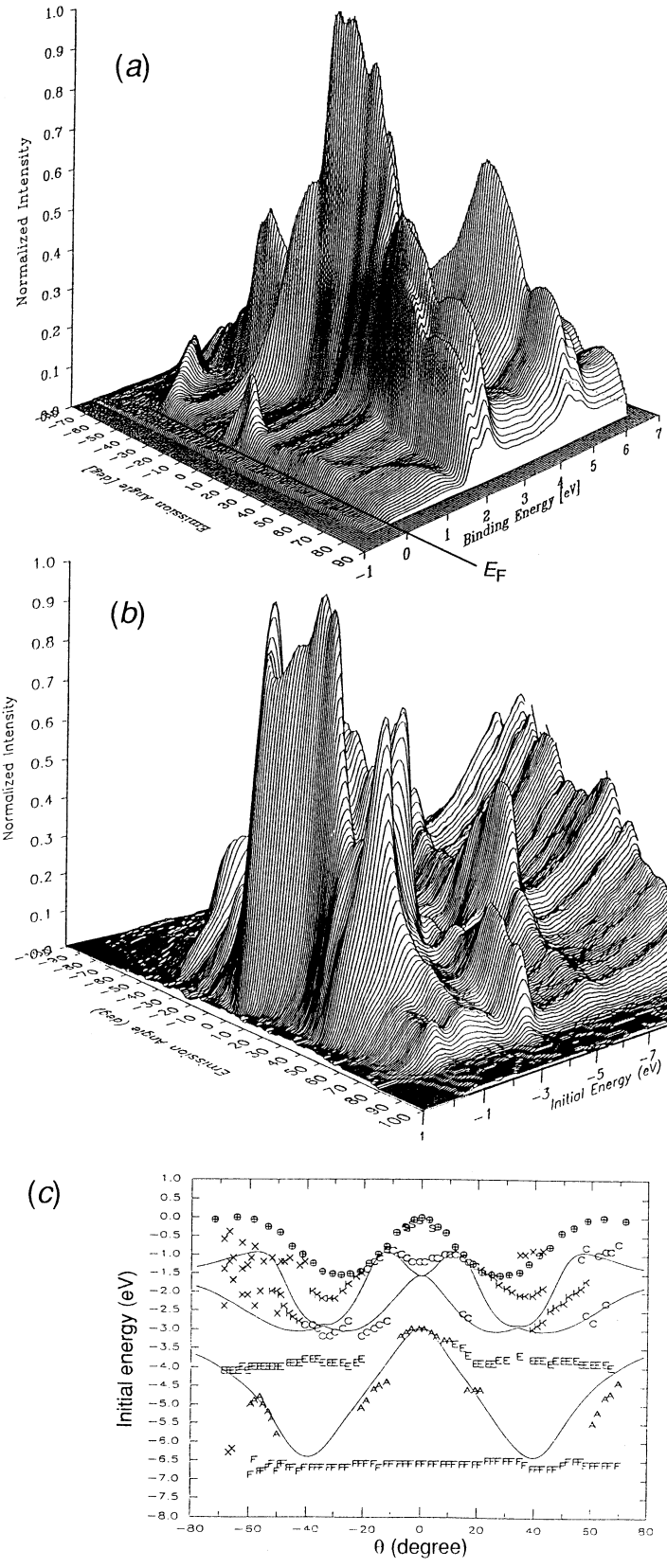
(a)
Normalized Intensity
Emission Angle [deg]
Binding Energy [eV]
E_F
(b)
Normalized Intensity
Emission Angle (deg)
Initial Energy (eV)
(c)
Initial energy (eV)
θ (degree)

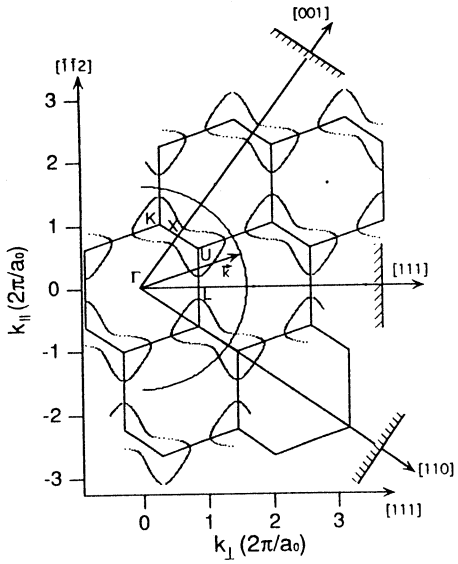

Fig. 5. A cut through the Fermi surface of Cu in a plane perpendicular to the [110] direction. The surface normals of three high-symmetry surfaces are indicated. The semicircle represents the final-state free-electron wavevector for electrons of kinetic energy 30 eV. (From Aebi *et al.* 1994.)

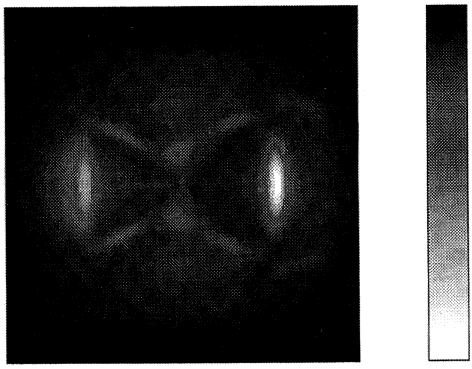

Fig. 6. Intensity of emission from the Fermi surface of a (110) surface of Cu illuminated at normal incidence with 24 eV p-polarised photons, drawn as a k_x–k_y plot as explained in the text.

For each azimuthal angle, the observed intensity relates to a projection onto the surface plane of a particular cut through the appropriate section of the bulk Fermi surface (see Fig. 5). As the azimuthal angle is scanned, this then illustrates the symmetry of the Fermi topology rather directly.

Two examples of such data are given in Figs 6 and 7. In Fig. 6, the photon energy has been selected to enhance emission from those parts of the Fermi surface of Cu which form the well-known 'dog's bone' shape. Since other projections of slices through the bulk Fermi surface may be readily obtained by altering the photon energy and the crystal surface used, the complete topology of the surface may be obtained (Aebi *et al.* 1993). The technique is inherently of less accuracy than the de Haas–van Alphen method, but is not subject to limitations due to impurity scattering and should consequently be of considerable use in the study of alloys.

Alternatively, by restricting the collection to a chosen azimuthal plane and increasing the detection energy in concert with the photon energy, so that the emission continues to originate from the Fermi energy, one may expect to observe directly the shape of the appropriate section of the Fermi surface. We consider

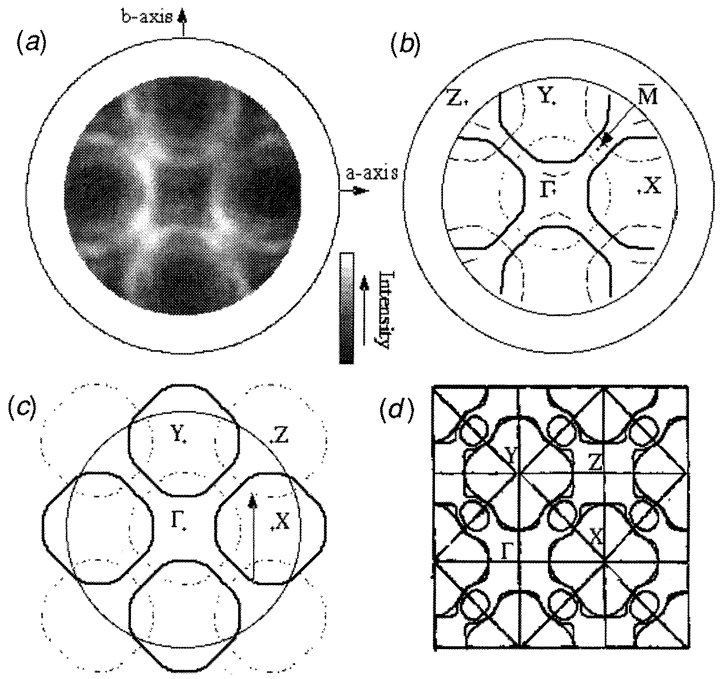

Fig. 7. (*a*) Intensity of emission from the Fermi surface of the Bi(2212) (001) surface, using 21·21 eV unpolarised photons. (*b*) Outline of (*a*) to assist in distinguishing the two emission patterns observable in the raw data. (*c*) Illustrating that the observed pattern may be constructed by means of a rigid shift of a single pattern by the ΓY distance. (*d*) The Fermi surface as calculated by Massidda *et al.* (1988). (From Aebi *et al.* 1994.)

that this constant initial state method will gain in popularity in the future as access to variable photon energies becomes more readily available.

Fig. 7 is a recent example of the manner in which the Fermi surface technique can be very directly applied to the study of quasi two-dimensional materials. The Fermi surfaces of many metals have been studied in recent years (Smith and Kevan 1991). The results shown in Fig. 7*a* (Aebi *et al.* 1994) are of additional significance in that they concern the contentious issue of the nature of the superconductivity of the alloy $Bi_2Sr_2CaCu_2O_{8+x}$. The shape of the Fermi surface predicted by a full-potential linearised augmented plane-wave calculation (Massidda *et al.* 1988) is shown in Fig. 7*d*; this calculation also predicts that the Fermi surface is largely constructed of states associated with the Cu–O planes, except for small electron surfaces around the M points from Bi–O derived bands. These latter features are missing from the experimental data which, however, can otherwise be matched closely if the main Fermi surface centred on Γ is replicated at all X and Y locations, as shown in Fig. 7*c*. The reduced size of the Brillouin zone implied by Fig. 7*c* requires the existence of a larger unit cell in real space than is appropriate for an unreconstructed surface. A $c(2 \times 2)$ superstructure is consistent with the observed periodicity in $\boldsymbol{k}$-space, strongly

suggesting local antiferromagnetic spin correlations in this (room-temperature) metallic phase (Aebi *et al.* 1994). This interpretation, if confirmed, would appear to have considerable significance for the theoretical treatment of the mechanism responsible for the superconductivity of this material.

5. Photoelectron Diffraction/Holography

Attempts have been made in recent years to determine details of the atomic structure in the surface region of crystalline solids using photoelectron diffraction. The most complete information (when only a single photon energy is available) comes from an examination of the intensity distribution of emission from a core photoelectron line covering the emission hemisphere, although restricted data sets (being sweeps in either polar or azimuthal angles) have often been used in the past (Egelhoff 1990). The traditional method of extracting structural information has been to perform scattering simulations using an assumed surface structure and to iteratively improve the agreement with experiment by modifying the structure. This is clearly a time-intensive procedure and considerable excitement was generated when it was proposed (Skoeke 1986) that the intensity map produced in a full hemisphere experiment could be regarded as a hologram and that the real-space structure in the neighbourhood of the emitting atom could be recovered by applying a phased Fourier transform procedure (Barton 1988). A number of attempts to confirm, or indeed to realise, this concept have appeared recently (Osterwalder *et al.* 1994) but the idea remains controversial.

The experiment itself is difficult only in the sense that some form of large-acceptance-angle analyser is required, and due to the fact that it has recently been established that multiple photon energy data sets are needed to reduce the presence of otherwise intense artifacts in the reconstructed hologram (Petersen *et al.* 1994). This clearly requires access to a synchrotron radiation facility, as the use of electron energies around 400 eV is indicated due to resolution requirements involving the de Broglie wavelength of the emitted electrons. It is the processing of the experimental data which is controversial, a variety of schemes having been proposed to overcome severe difficulties involving non-physical artifacts which are apparent when a phased Fourier transform is applied to a single data set, as originally proposed (Barton 1988).

As an example of a successful multiple photon energy study, Fig. 8 shows a comparison between a holographically reconstructed image showing eight atoms belonging to three atomic layers near the surface of a Pt crystal and their expected positions. These data are from an IBM group (Petersen *et al.* 1994) and were obtained at the Brookhaven source using a summation of eight full-hemisphere Pt 4f electron intensity distributions. The authors claim a positional accuracy of $\pm 0 \cdot 3$ Å for the location of the atomic positions (parallel to the surface) from this reconstruction, sufficient to provide an excellent starting point for a more accurate determination using iterative scattering calculations, even though the perpendicular resolution is much worse ($\pm 1 \cdot 5$ Å) due largely to the limited electron energy (wavevector) range used.

This experiment is of significance as it appears to demonstrate the applicability of the technique to near-surface structural determinations; previously, it had been thought that the method would only hold promise for the study of adsorbate structures.

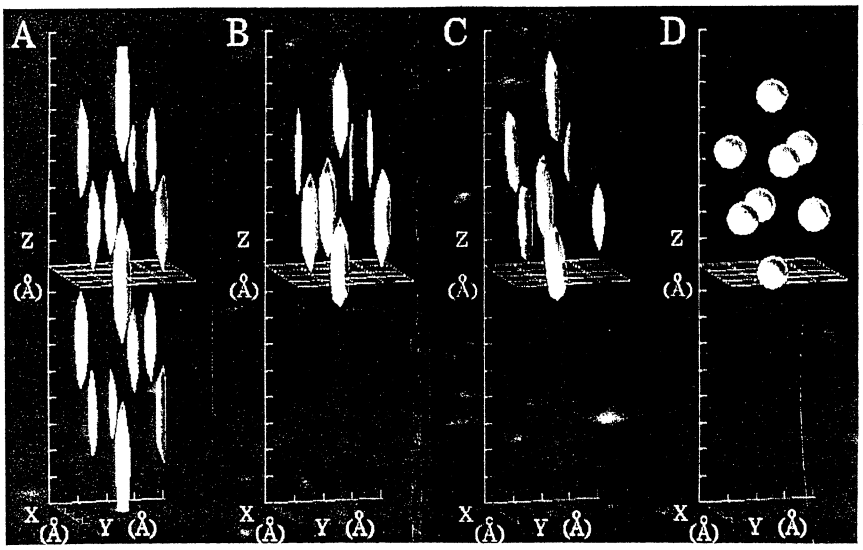

Fig. 8. Iso-density real-space images showing side views of eight atoms of a Pt crystal holographically reconstructed from Pt 4f photoemission data. Panel A shows the image reconstructed from single photon energy data, including the twin image. Panels B and C show the image resulting from two different reconstruction procedures involving eight photon energy data sets, while panel D illustrates the theoretically expected atomic positions. (From Petersen *et al.* 1994.)

An alternative reconstruction algorithm, which requires the acquisition of data as a function of photoelectron momentum for a restricted set of emission directions, has also been sucessfully employed in a study of the Si(111) Al system (Wu *et al.* 1994). This approach may be considered as a form of vector EXAFS (extended X-ray absorption fine structure) and is an extension of the technique known as scanned energy photoelectron diffraction, as practiced by Woodruff *et al.* for example (see Dippel *et al.* 1992). In this study, the intensity of the Al 2p level was measured at a set of photon energies calculated to provide equal increments in photoelectron momentum, and the data then inverted into a real-space representation. This procedure was repeated for a selection of polar and azimuthal emission angles and the inverted data sets summed to decrease the intensity of artifacts introduced due to the (often considerable) phase shifts occurring at each atomic scattering event. The resulting reconstructions are of high quality and show, in a very direct way, the local geometry of the emitting Al atom.

The two examples highlighted above give hope that the holographic technique is developing into a useful method for at least preliminary estimation of surface structure. The initial optimism following the Skoeke and Barton papers has necessarily been tempered by the realisation that the volume of phase space sampled in a single energy hologram is insufficient to reconstruct a reliable real-space image, and that such images are likely to be dominated by artifacts and by the twin image problem (Chambers 1992). It now appears clear that the most successful reconstructions will be those in which the data set obtained includes as

many emission angles and photoelectron momenta as possible. Such measurements represent a considerable investment in synchrotron radiation beamtime and may only be justified in those cases where no other method has been shown to be successful.

6. Quantum Size Effects

Surface scientists have always worked in the nanometre region in the sense that monolayers, or for that matter surface states, demonstrate spatial confinement measured in Ångstroms, although only in one dimension. As an example of the utility of the photoemission technique for the investigation of the electronic properties of quantum dots, we may refer to the data of Fig. 9. Here the behaviour of thin layers of Ag evaporated on GaAs(110) at liquid nitrogen temperatures has been exploited to form pyramidal islands with nanometre dimensions, when the layers are allowed to reconstruct by warming to room temperature (Evans *et al.* 1993).

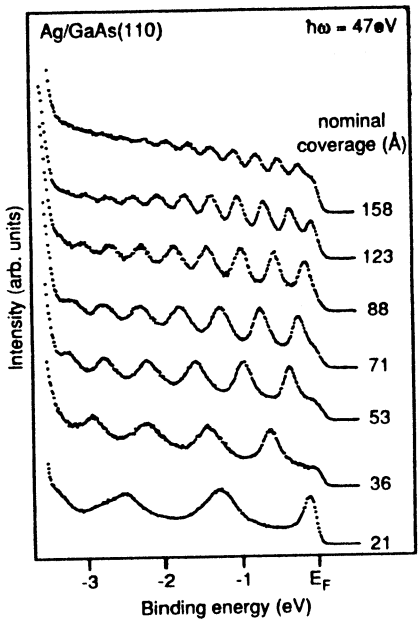

Fig. 9. Valence photoelectron spectra of seven Ag layers of thickness indicated, prepared by deposition at 100 K and subsequently annealed to room temperature. Spectra were recorded at a polar angle of 25° with respect to the surface normal along the [111] azimuth of the GaAs(110) surface. (From Evans *et al.* 1993.)

Evidence for the spatial confinement of the electrons within these islands may clearly be seen as regular intensity variations in the energy distribution curves of Fig. 9. These data show a region which is well known to be a featureless plateau for the case of disordered, bulk Ag. The intensity variations depend on the nominal thickness of the cold-deposited films (and consequently on the size of the annealed islands as determined by scanning tunnelling microscopy) and are related to the angle of emission of the detected electrons. This latter observation may be correlated with the facets of the pyramidal islands. Since a distribution in crystallite island size is inevitable given the growth conditions, an analysis of the confined electronic states involved is somewhat compex and the reader is referred to the original paper for further detail (Evans *et al.* 1993).

7. Investigation of Magnetic Sub-levels

Much valuable work has been performed on magnetic materials using plane-polarised synchrotron radiation produced by the bending magnets of a storage ring in conjunction with energy- and spin-selected electron spectroscopy (Kirschner 1985). Such experiments have the advantage that they distinguish magnetic sub-levels but, despite advances in the efficiency of spin analysis techniques, remain difficult because of the complexity of the apparatus and low count rates.

Circularly polarised radiation is available just below and just above the plane of the orbit from bending magnets, but the intensity of this radiation falls off rapidly due to the small vertical divergence of the beam (Koch *et al.* 1983). More recently, intense circularly polarised radiation has been produced from a pair of orthogonal undulators placed in a straight section of a storage ring

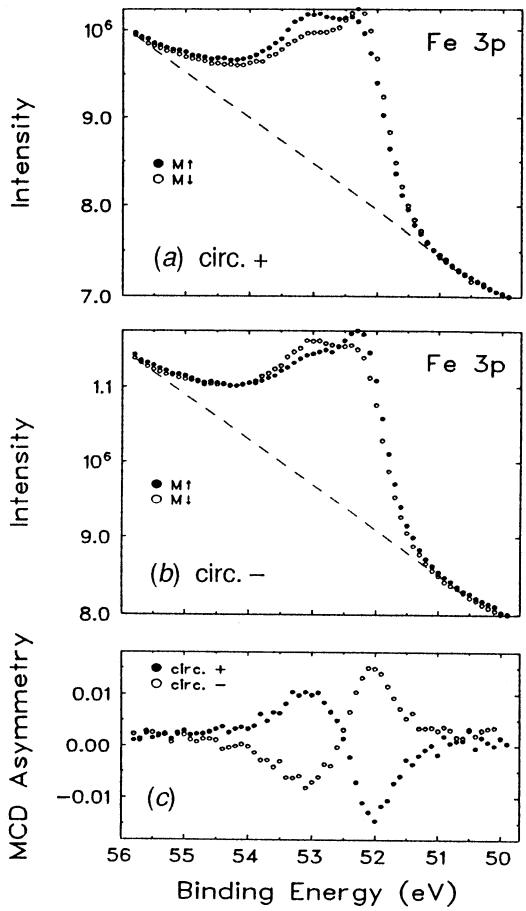

Fig. 10. Magnetic circular dichroism from the Fe 3p core level obtained using a 90 eV photon energy: (*a*) Fe 3p intensity using circularly polarised light with remanent magnetisation parallel and antiparallel to [100]; (*b*) as for (*a*) but using light of opposite helicity; and (*c*) asymmetry curves obtained using data of (*a*) and (*b*). (From Roth *et al.* 1992.)

(Bahrdt *et al.* 1992). The helicity of the radiation can be adjusted using a phase shifter inserted between the undulators, thereby opening up the possibility of using magnetic circular dichroism as a means of investigating the magnetic levels in many materials, i.e. the technique is not restricted to those with permanent moments (Schonhense 1990).

The availability of both right and left circularly polarised radiation implies that there is no longer a need to spin-select the emitted photoelectrons following energy selection in order to identify the spin-up/spin-down components of a particular photoelectron line. This is a considerable simplification in terms of instrumentation whereas the intensity of the undulator radiation further assists the investigator.

A recent example of the use of the technique of magnetic circular dichroism (MCD) is shown is Fig. 10 for the case of the 3p level in Fe. This work used the BESSY facility to investigate the effects of altering the direction of magnetisation of a thin film of Fe on an Ag(100) substrate in conjunction with the sign of the helicity of the incident light (Roth *et al.* 1992). Since the photons were incident at 16° from the surface plane, the projection of the helicity could be arranged to be either parallel or antiparallel to the direction of remanent magnetisation of the sample. The MCD effect is clearly apparent in the doublet form of the line, which is attributed to the joint effect of spin–orbit and exchange interactions of almost equal strength.

8. Conclusion

A brief survey of certain selected results using the technique of angle-resolved photoelectron spectroscopy in conjunction with synchrotron radiation has been provided. The data have been selected arbitrarily in line with the authors' interests and are not necessarily representative of much excellent work being performed in other fields. One of the better methods of surveying the type of experiment which is of particular current interest at any time is to examine the yearbooks published by each of the synchrotron radiation facilities. A list of these may be found in the journal *Synchrotron Radiation News*.

Acknowledgments

The work described above, other than that directly referenced, is the result of a long-standing collaboration between La Trobe University and the University of Erlangen-Nürnberg, Germany. Many present and past students have contributed to the success of this collaboration, including Y. Q. Cai, Z. D. Zhang, A. J. P. Stampfl, R. Denecke, J. Faul, and J. ConFoo. We express our gratitude to Proessor P. Aebi, Universite de Fribourg, Switzerland, for providing Fig. 7. We also acknowledge financial assistance from the Australian Research Council, and to the 'Access to Major International Facilities' and the 'Bilateral Science and Technology' programs of the Department of Industry, Science and Technology.

References

Aebi, P., Osterwalder, J., Fasel, R., Naumovic, D., and Slapbach, L. (1993). *Surf. Sci.* **307–9**, 917.

Aebi, P., Osterwalder, J., Schwaller, P., Slapbach, L., and Shimoda, M. (1994). *Phys. Rev. Lett.* **72**, 2757.

Bahrdt, J., Gaupp, A., Gudat, W., Mast, M., Molter, K., Peatman, W. B., Scheer, M., Schroeter, Th., and Wang, Ch. (1992). *Rev. Sci. Instrum.* **63**, 339.
Barton, J. J. (1988). *Phys. Rev. Lett.* **61**, 1356.
Cai, Y. Q. (1992). Ph.D. Thesis, La Trobe University (unpublished).
Chambers, S. A. (1992). *Surf. Sci. Rep.* **16**, 261.
Christensen, N. E. (1984). *Phys. Rev.* B **30**, 5753.
Dippel, R., Woodruff, D. P., Hu, X-M., Asensio, M. C., Robinson, A. W., Schindler, K-M., Weiss, K-U., Gardiner, P., and Bradshaw, A. M. (1992). *Phys. Rev. Lett.* **68**, 1543.
Egelhoff, W. F., Jr (1990). *Crit. Rev. Solid State Mater. Sci.* **16**, 213.
Evans, D. A., Alonso, M., Cimino, R., and Horn, K. (1993). *Phys. Rev. Lett.* **70**, 3483.
Himpsel, F. J. (1983). *Adv. Phys.* **32**, 1.
Hufner, S. (1994). 'Photoelectron Spectroscopy, Principles and Applications', Springer Series in Solid State Science, Vol. 82 (Springer: Berlin).
Jenkin, J. G., Leckey, R. C. G., and Liesegang, J. (1977). *J. Electron Spectrosc. Relat. Phenom.* **12**, 1.
Kirschner, J. (1985). 'Polarized Electrons at Surfaces', Springer Tracts in Modern Physics, Vol. 106 (Springer: Berlin).
Koch, E.-E., Sasaki, T., and Winick, W. (Eds) (1983). 'Handbook of Synchrotron Radiation' (North Holland: Amsterdam).
Leckey, R. C. G., and Riley, J. D. (1992). *Crit. Rev. Solid State Mater. Sci.* **17**, 307.
Massidda, S., Jaejun, Yu, and Freeman, A. J. (1988). *Physica* C **158**, 251.
Osterwalder, J., Fasel, R., Stuck, A., Aebi, P., and Slapbach, L. (1994). *J. Electron Spectrosc. Relat. Phenom.* **68**, 1.
Petersen, H. J., Gudat, W., Hellwig, C., Jung, C., and Peatman, W. (1991). Jaresbericht, Berliner Electronenspeicherring-Gesellschaft für Synchrotronstrahlung mBH, p. 478.
Petersen, H., Jung, C., Hellwig, C., Peatman, W., and Gudat, W. (1992). Jaresbericht, Berliner Electronenspeicherring-Gesellschaft für Synchrotronstrahlung mBH, p. 494.
Petersen, B. L., Terminello, L. J., Barton, J. J., and Shirley, D. A. (1994). *Chem. Phys. Lett.* **220**, 46.
Roth, Ch., Hillebrecht, F. U., Rose, H., Kisker, E., Finazzi, M., and Braicovich, L. (1992). Jaresbericht, Berliner Electronenspeicherring-Gesellschaft für Synchrotronstrahlung mBH, p. 214.
Schonhense, G. (1990). *Phys. Scripta* **T31**, 255.
Skoeke, A. (1986). 'Short Wavelength Coherent Radiation: Generation and Applications', AIP Conf. Proceedings No. 147 (American Institute of Physics: New York).
Smith, K. E., and Kevan, S. D. (1991). *Phys. Rev.* B **43**, 3986.
Wu, H., Lapeyre, G. J., Huang, H., and Tong, S. Y. (1994). *Phys. Rev. Lett.* (in press).
Zhang, X. D., Riley, J. D., Leckey, R. C. G., and Ley, L. (1993). *Phys. Rev.* B **48**, 17077.

Manuscript received 6 July, accepted 21 October 1994